Volume 9
Number 33
7 September 2021
Pages 6483–6704

Journal of Materials Chemistry B

Materials for biology and medicine

rsc.li/materials-b

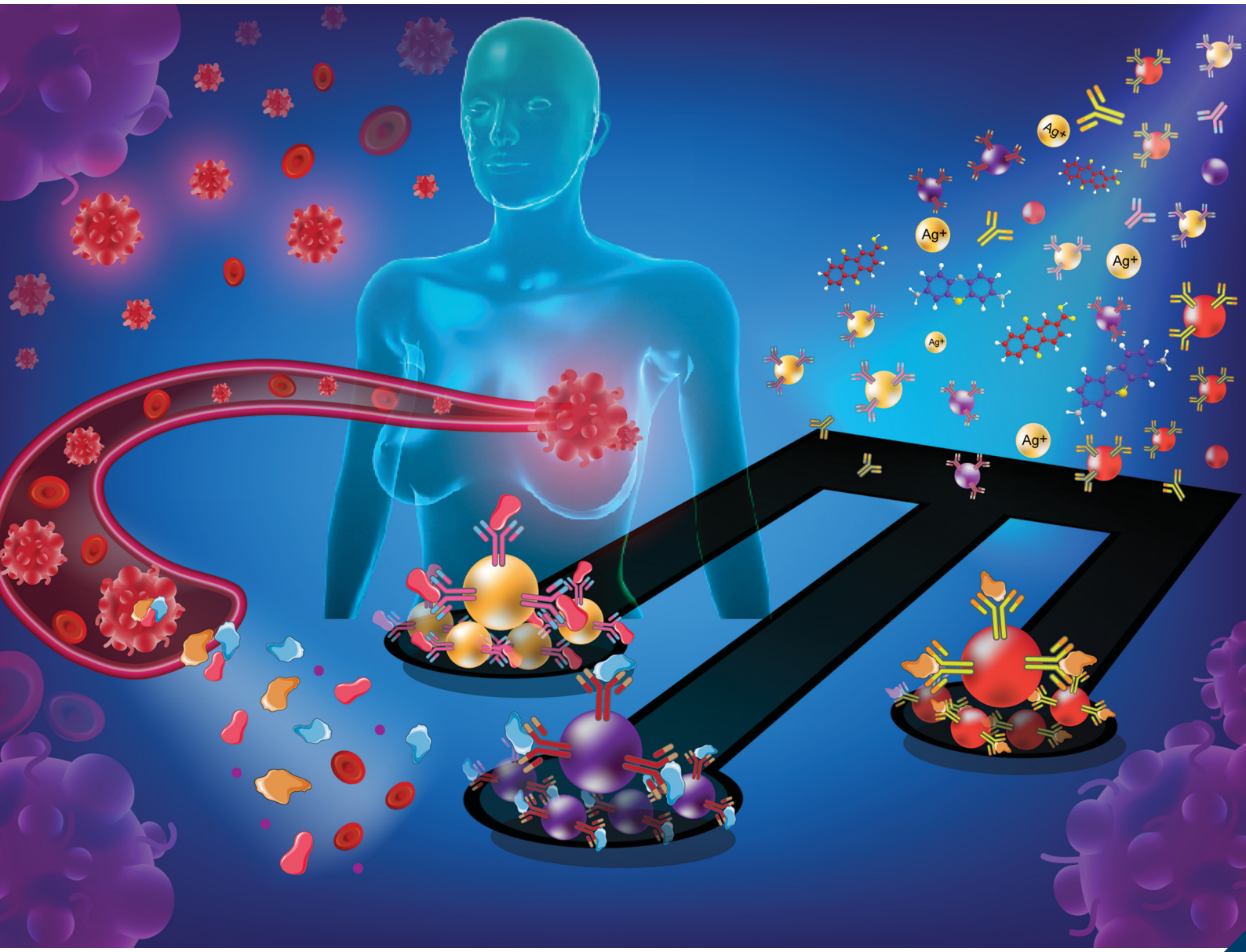

ISSN 2050-750X

ROYAL SOCIETY OF CHEMISTRY

PAPER

Kontad Ounnunkad *et al.*

A label-free multiplex electrochemical biosensor for the detection of three breast cancer biomarker proteins employing dye/metal ion-loaded and antibody-conjugated polyethyleneimine-gold nanoparticles

Indexed in Medline!

Journal of Materials Chemistry B

ROYAL SOCIETY OF CHEMISTRY

PAPER

View Article Online
View Journal | View Issue

Cite this: J. Mater. Chem. B, 2021, 9, 6576

A label-free multiplex electrochemical biosensor for the detection of three breast cancer biomarker proteins employing dye/metal ion-loaded and antibody-conjugated polyethyleneimine-gold nanoparticles†

Kulrisa Kuntamung,[ab] Jaroon Jakmunee [acde] and Kontad Ounnunkad [*acde]

A new electrochemical immunosensor is developed for the label-free simultaneous detection of mucin1 (MUC1), cancer antigen 15-3 (CA15-3), and human epidermal growth factor receptor 2 (HER2) early breast cancer biomarkers. The biosensor is simply designed using the deposition of three different systems of redox species-antibody-conjugated polyethylenimine coated-gold nanoparticles (PEI-AuNPs), for the first time. The screen-printed carbon electrode (SPCE) comprising a three-working electrode array is modified with the conjugated PEI-AuNPs. Multiplex sensing is performed by utilizing the distinguishable electrochemical responses of the redox-active species; anthraquinone-2-carboxylic acid (AQ), thionine chloride (TH), and $AgNO_3$ (Ag^+) on the PEI-AuNPs conjugates for the detection of MUC1, CA15-3, and HER2, respectively. The single-run determination of the biomarkers by the proposed immunosensor is carried out by measuring the decrease (%) in the oxidation peak currents due to the formation of three kinds of antibody-antigen complexes. The decreased currents are logarithmically proportional to the antigen concentrations in the ranges of 0.10–100 U mL^{-1} CA15-3 and 0.10–100 ng mL^{-1} MUC1 and HER2 with detection limits of 0.21 U mL^{-1}, 0.53 ng mL^{-1} and 0.50 ng mL^{-1}, respectively, which are significantly lower than the clinically relevant cut-off levels. The sensor reveals high selectivity and satisfactory reproducibility. After storing for two weeks, the sensor retains the responses with *ca.* 90% of the initial currents. The immunosensor is successfully applied to detect three tumor markers in human serum and can provide a new technological platform for the development of low-cost, highly stable, sensitive, selective, and point-of-care (POC) diagnosis.

Received 26th April 2021,
Accepted 29th June 2021

DOI: 10.1039/d1tb00940k

rsc.li/materials-b

Introduction

Breast cancer is one of the most leading causes of mortality in women worldwide, accounting for more than two million cases each year.[1–3] Even though breast cancer often occurs in females, about 1% of all breast cancers is found in males.[4] Most patients with breast cancer are diagnosed at a late stage, which makes the treatment much more difficult and costly than those before symptoms appear.[5] If cancer is found at an early stage, it can be controlled and treated successfully, improving the chance of patient survival.[5,6] Assays of tumor markers have been shown to offer new hope for early detection of breast cancer.[7] There are various biomarkers recommended to identify breast cancer.[8] Among these biomarkers, patients with breast cancer typically show the positive expression of three tumor markers: mucin1 (MUC1),[9–11] cancer antigen 15-3 (CA15-3),[12–14] and human epidermal growth factor receptor 2 (HER2),[15] which are often applied in early diagnosis. Only a single biomarker measurement is insufficient to ensure an accurate diagnosis because most biomarkers are not specific for a particular cancer, and most cancers have more than one tumor marker.[16,17] For instance, carcinoembryonic antigen is associated with lung, pancreatic, liver, breast, ovarian, and colorectal cancers, while alpha-fetoprotein is usually relevant to liver cancer and epithelial ovarian tumors.[17,18] In order to accurately and reliably diagnose cancer at early stages, the simultaneous determination of

[a] Department of Chemistry, Faculty of Science, Chiang Mai University, Chiang Mai 50200, Thailand. E-mail: suriyacmu@yahoo.com, kontad.ounnunkad@cmu.ac.th
[b] The Graduate School, Chiang Mai University, Chiang Mai 50200, Thailand
[c] Center of Excellence for Innovation in Chemistry, Faculty of Science, Chiang Mai University, Chiang Mai, 50200, Thailand
[d] Research Center on Chemistry for Development of Health Promoting Products from Northern Resources, Chiang Mai University, Chiang Mai, 50200, Thailand
[e] Center of Excellence in Materials Science and Technology, Chiang Mai University, Chiang Mai 50200, Thailand

† Electronic supplementary information (ESI) available. See DOI: 10.1039/d1tb00940k

several cancer biomarkers is of great interest in clinical diagnosis.[19,20] Additionally, it can improve the test efficiency, shorten the analytical time, decrease the sampling volume and reduce cost.[21,22]

Among various analytical techniques for the detection of cancers, electrochemical immunosensors have received much attention in multiple markers analysis due to their high sensitivity, simple instrumentation, good portability, and cost-effectiveness.[23,24] Typically, the multiplex electrochemical immunosensor is of two main types: multiplex sandwich and label-free types.[25] For the multiplex sandwich-type, it is mainly focused on multiple labels/tags with secondary antibodies, corresponding to the multi-analyte detection.[22,26] This method provides high sensitivity and low limit of detection (LOD); however, there are some limitations because of the use of secondary-antibody labeling being operated with multiple steps, cross reactivity due to adjacent redox probes, and time-consuming procedures.[21,22,27] The detection based on label-free type solves these disadvantages which offers simple handling, low price, and measurement without the complicated labeling process.[28] There are many reports about the successfully developed simultaneous detection of multiple markers, but it is still a challenge to explore novel approaches to improve the device's simplicity and sensitivity. In addition, bioconjugates are commonly used in sandwich systems; however, to the best of our knowledge, there is no report about their usage in label-free detection. Thus, the bioconjugates containing both signaling molecules and antibodies offer an easy alternative to develop a new platform based on label-free type for the simultaneous detection of multiple markers, which greatly simplifies and is demonstrated with a shorter time of the device fabrication process. In bioconjugation designs for the multiplex electrochemical immunosensor, attachment of the redox-active species plays an important role in generating distinguishable signals for multiple biomarker detection. To date, the widely employed redox-active species are metal ions such as Zn^{2+}, Cd^{2+}, Cu^{2+} and Pb^{2+}, and organic dyes such as thionine, Prussian blue and methylene blue.[29,30] Interestingly, anthraquinone-2-carboxylic acid (AQ), thionine chloride (TH), and $AgNO_3$ (Ag^+) can produce three distinctive and distinguishable signals in a single run. Another crucial factor for electrode fabrication is the immobilization of antibodies and adsorption of redox-active species. Various materials have been used for loading numerous redox active species as well as proteins such as gold nanoparticles (AuNPs),[29] carbon nanomaterials,[24,31] and magnetic beads.[32] Among them, AuNPs have attracted interest due to their good electrical conductivity, massive surface area, strong adsorption ability, and biocompatibility.[33] Since the AuNPs tend to agglomerate easily, polyethyleneimine (PEI) can effectively improve the stability of the AuNPs.[34] Interestingly, poly(ethyleneimine)-coated-AuNPs (PEI-AuNPs) not only provide stability in practical use but also help in binding efficiency with many kinds of materials, *i.e.*, signaling molecules, antibodies, and proteins. The amino groups of PEI on AuNPs offer electrostatic interaction with both biomolecules and redox-active species and also preserve the biomolecular activity.[34,35] In previous studies, PEI-AuNPs were used as labeling tags in an electrochemical sensor for multiplex immunoassay, which can improve detection efficiency and achieve high sensitivity.[35] Therefore, PEI-AuNPs are an interesting nanomaterial for absorbing antibodies and the signal-generation species to construct the sensor.

Herein, we developed a new multiplex label-free electrochemical immunosensor to determine three breast cancer biomarkers (*e.g.*, MUC1, CA15-3, and HER2). The present work reports the fabrication of a multiplex label-free immunosensor with a single test by the use of three different redox species adsorbed on PEI-AuNPs as three signal amplifiers, on which individually conjugated different antibodies. The resultant three different redox probe-antibody PEI-AuNPs were directly deposited on a three-screen-printed carbon electrode (3-SPCE) array for multiplex detection of the corresponding target biomarkers. Additionally, the designed immunosensor achieves high specificity (each array electrode acts independently to detect each specific antigen/target analyte), good reproducibility, and convenience to be operated. Furthermore, the simultaneous determination of MUC1, CA15-3, and HER2 by our sensor is successfully applied in human serum and is a suitable approach for the early diagnosis of breast cancer with high precision.

Experimental section

Materials

CA15-3 protein (lot: A17091310), CA15-3 antibody (lot: M002204), and alpha-fetoprotein (AFP, lot: A16042812, 6.9 mg mL^{-1}, >98%) were purchased from Fitzgerald Industries International (USA). Recombinant human HER2/ErbB2 protein (lot: LC11MC0201), HER2/ErbB2 antibody (lot: HB07AP2810-B), recombinant human MUC1/Mucin1 protein (lot: LC08JA2304), and MUC1/Mucin1 antibody (lot: HB10MA2801-B) were obtained from Sino Biological Inc. (China). Anthraquinone-2-carboxylic acid (AQ, 98%) and thionine chloride (TH, ≥98%) were purchased from Sigma-Aldrich (Japan). Silver nitrate ($AgNO_3$, ≥99.7%), sodium acetate ($CH_3COONa{\cdot}3H_2O$, 99.1%), and sodium dihydrogen phosphate dihydrate ($NaH_2PO_4{\cdot}2H_2O$, 99.0–101.0%) were obtained from Fisher Scientific (USA). Polyethylenimine (PEI, branched, $M_w \approx 800$) and gold(III) chloride hydrate ($HAuCl_4{\cdot}xH_2O$, 99.999% trace metals basis) were bought from Sigma-Aldrich (Singapore). Recombinant human GM2A protein (GM2AP, lot: E32211-8929) was purchased from Abcam (USA). Alpha-fetoprotein (AFP, lot: A16042812, 6.9 mg mL^{-1}, >98%) was obtained from Fitzgerald Industries International (USA). Disodium hydrogen phosphate dihydrate ($Na_2HPO_4{\cdot}2H_2O$, 99.5%), potassium ferricyanide ($K_3[Fe(CN)_6]$, 99%), acetic acid (99.7%), interleukin-15 (IL-15, lot: 2381730, ≥98%), dopamine hydrochloride (DA, 98%), and bovine serum albumin (BSA, lot: D00155527, 98%) were purchased from Qrec (Newzealand), Merck (Germany), RCI Labscan (Thailand), Millipore (USA), Sigma-Aldrich (Germany), and Calbiochem (USA), respectively. D-(+)-glucose (Glu, ≥99.5%), L-ascorbic acid (AA, 99%), phosphate-buffered saline (PBS) tablets (pH 7.4), potassium hexacyanoferrate(II) trihydrate ($K_4[Fe(CN)_6]{\cdot}3H_2O$, 99%), anti-Human IgG (Fab specific) antibody produced in goat (lot: 112M4812V, 5.5 mg mL^{-1}),

immunoglobulin G (IgG, lot: 082M4772V, 4.8 mg mL^{-1}, ≥95%), and human serum from human male (AB plasma, USA origin, lot: SLBS6544) were purchased from Sigma-Aldrich (USA).

Apparatus

The morphology and structure of the nanocomposites were characterized using a transmission electron microscope (TEM, JEM-2010, Japan) and a scanning electron microscope (FE-SEM, JSM-6335F, Japan). UV-Visible (UV-vis) spectra of PEI-AuNPs were recorded using an Evolution 201 Spectrophotometer (Thermo Scientific, USA). Centrifugation was performed using a Digicen 21 (Orto alresa, Spain). The mixture solution was shaken on a thermomixer (Eppendorf, Germany). Electrochemical experiments including cyclic voltammetry (CV) and square wave voltammetry (SWV) were performed using an EmStat3 Potentiostat (PalmSens, Netherlands). Electrochemical impedance spectroscopy (EIS) measurement was carried out using a PalmSens4 Potentiostat (PalmSens, Netherlands). The electrochemical measurements were performed in an electrochemical cell consisting of a three-electrode system, *i.e.*, a 3-SPCE array as a working electrode, a platinum wire as an auxiliary electrode, and an Ag/AgCl electrode (3 M NaCl) as a reference electrode. The diameter of each electrode of an SPCE array is 3.0 mm in size. Fourier transform infrared (FT-IR) spectra were recorded using a Bruker Tensor 27 FT-IR instrument (Germany). Thermogravimetric analysis (TGA) was performed on a Thermo plus EVO 2 instrument (TG-DTA 8122, Rigaku Corp., Japan).

Preparation of PEI-AuNPs

The PEI-AuNPs used in this work were prepared according to the previous procedure with some modifications.[35] Briefly, 0.90 mL of 1.0% w/v PEI solution, which acts as a reducing agent as well as a stabilizing agent, was added into 25.00 mL of 1.40 mM $HAuCl_4$ aqueous solution in a round bottom flask under a magnetic stirring rate of 800 rpm for 16 h. The resulting wine-red solution was then centrifuged at 6000 rpm for 10 min to achieve a sediment product. The obtained sediment was dispersed and adjusted with DI water to obtain 50 mL of dispersion. Finally, the PEI-AuNP solution was stored at 4 °C until further use.

Preparation of redox species-antibody-conjugated PEI-AuNPs

The preparation of redox species-antibody-conjugated PEI-AuNPs is exhibited in Scheme 1A. Three kinds of redox species-antibody-conjugated PEI-AuNPs were individually prepared. First, 2.0 μL of each antibody solution (60 μg mL^{-1}) was injected into 50.0 μL of PEI-AuNPs and then incubated in a thermomixer at 400 rpm at 25 °C for 1 h. After incubation, the antibodies were attached to PEI-AuNPs. The antibody-conjugated PEI-AuNP solutions were centrifuged at 5500 rpm for 10 min to remove the unbound antibodies. The obtained antibody-PEI-AuNPs were washed with 50.0 μL of DI water by centrifugation at 4800 rpm for 10 min. After that, the antibody-PEI-AuNP product was added with 50.0 μL of 10 mM AQ, 10 mM TH, or 0.5 mM Ag^+ solution and mixed in a thermomixer at 400 rpm at 25 °C overnight to adsorb dyes/Ag^+ ions on bioconjugate PEI-AuNPs. Finally, the dye/Ag^+ ion-antibody-PEI-AuNP solutions were centrifuged at 4800 rpm for 10 min and then washed with 50.0 μL of DI water. Then, each of the three products was separated by centrifugation at 4800 rpm for 10 min. Each product was redispersed with 50.0 μL of DI water and then kept at 4 °C for further use. Three prepared redox PEI-AuNP-based conjugate systems, comprising of AQ-anti-MUC1-PEI-AuNPs, TH-anti-CA15-3-PEI-AuNPs, and Ag^+-anti-HER2-PEI-AuNPs, were employed for the multiplex detection of MUC1, CA15-3, and HER2, respectively.

Fabrication of the immunosensor

The fabrication procedure of the label-free electrochemical immunosensor is shown in Scheme 1B. Firstly, 5.0 μL of each dye/metal ion-antibody-PEI-AuNP solution was added dropwise on each electrode of a plasma-cleaned 3-SPCE array. Then, three modified areas of the array were incubated with a blocking solution containing 0.05% w/v BSA for 30 min to eliminate the non-specific binding sites between the proteins and electrode array surfaces, followed by washing with a PB buffer

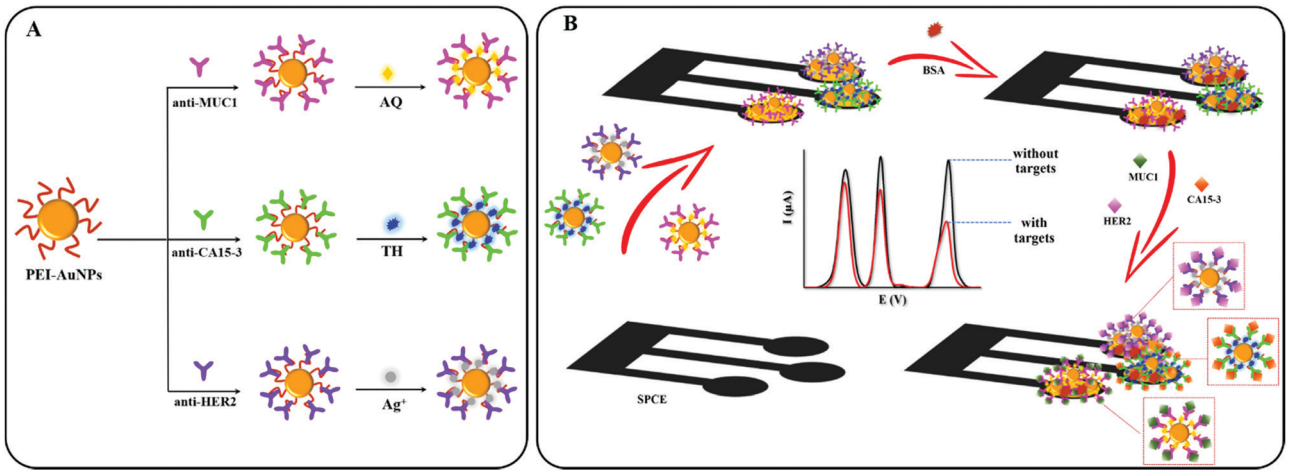

Scheme 1 (A) The preparation procedure of AQ-anti-MUC1-PEI-AuNPs, TH-anti-CA15-3-PEI-AuNPs, and Ag^+-anti-HER2-PEI-AuNPs and (B) the fabrication procedure of the multiplex label-free electrochemical immunosensor.

(1 mM, pH 7.0) several times. The fabricated immunosensor was finally obtained and stored at a temperature of 4 °C before the simultaneous assay.

Electrochemical measurement

For the immunoassay, the prepared immunosensor was incubated with three types of tumor marker standard solutions (MUC1, HER2, and CA15-3) for 30 min at room temperature and, to remove the unabsorbed antigen, followed by washing with a PB buffer three times. To construct the calibration curves, the three immunosensing surfaces capture the biomarker proteins by varying MUC1 and HER2 concentrations of 0.10–100 ng mL^{-1} and CA15-3 concentration of 0.10–100 U mL^{-1}. Finally, three well-discriminated voltammetric peaks, belonging to electrochemical responses of three redox probes as well as three different cancer biomarkers, were carried out using SWV in contact with an acetate buffer solution (0.20 M, pH 5.0). The SWV measurement was performed with the potential range from −1.1 V to 0.8 V, a step potential of 4.0 mV, a frequency of 15 Hz, and an amplitude of 25 mV. The CV and EIS measurements were employed to monitor the stepwise fabrication processes of the immunosensor in 0.010 M PBS (pH 7.4) containing 5.0 mM $[Fe(CN)_6]^{3-/4-}$. The CV measurements were carried out by scanning the potential in the range from −0.40 to 0.80 V at a scan rate of 50 mV s^{-1} while the EIS measurements were recorded at a frequency ranging from 10^{-1} to 10^5 Hz with an alternating current voltage amplitude of 10 mV.

Results and discussion

Characterization of redox species-antibody-conjugated PEI-AuNPs

For the development of redox bioconjugate particles, an anti-IgG antibody was employed as a model antibody to study its binding and attachment of redox probes on PEI-AuNPs. The formation of redox species-antibody-conjugated PEI-AuNPs was investigated by UV-vis spectroscopy, as shown in Fig. S1 (ESI†). The spectrum of PEI-AuNPs exhibits a maximum absorption peak at 523 nm (curve a), which is ascribed to the SPR band of AuNPs. After the PEI-AuNPs are conjugated to antibody (curve b), only the characteristic absorbance of PEI-AuNPs reveals no significantly observable difference in shape and maximum absorbance when compared to that of starting PEI-AuNPs. This implies that there is no agglomeration during the conjugation process. From curve c, three strong absorption peaks at 210, 258, and 334 nm are observed for pure AQ. When AQ is attached to antibody-PEI-AuNPs, we observe its absorption peaks together with an absorption peak at 523 nm from PEI-AuNPs (curve d), indicating that an AQ-antibody-PEI-AuNP bioconjugate is successfully formed. The absorption peak at 598 nm is observed for pure TH (curve e). TH is labeled onto antibody-PEI-AuNPs; however, we only observe one absorption peak at 598 nm (curve f). The peak derives from the peak overlapping of TH and PEI-AuNPs. Moreover, the absorption peak of Ag^+ is observed at 206 nm (curve g), while one characteristic peak at 523 nm is obtained for the Ag^+-antibody-PEI-AuNPs (curve h). This result confirms that the redox species-antibody-conjugated PEI-AuNPs are successfully formed. Moreover, the FT-IR spectra (Fig. S2, ESI†) and TGA profiles (Fig. S3, ESI†) also confirm the formation of the products. For the determination of MUC1, CA15-3, and HER2, three kinds of redox bioconjugate particles, namely AQ-anti-MUC1-PEI-AuNPs, TH-anti-CA15-3-PEI-AuNPs, and Ag^+-anti-HER2-PEI-AuNPs, were prepared for fabrication of immunosensing surfaces.

The structural properties such as size and morphology of redox species-antibody-conjugated PEI-AuNPs are analyzed through TEM measurement, as presented in Fig. 1. The prepared PEI-AuNPs are almost spherical particles without particle aggregation. The average diameter is approximately 13.7 nm (Fig. 1A), which provides a high surface area for immobilizing active molecules and redox species. After the attachment of antibody and dye/

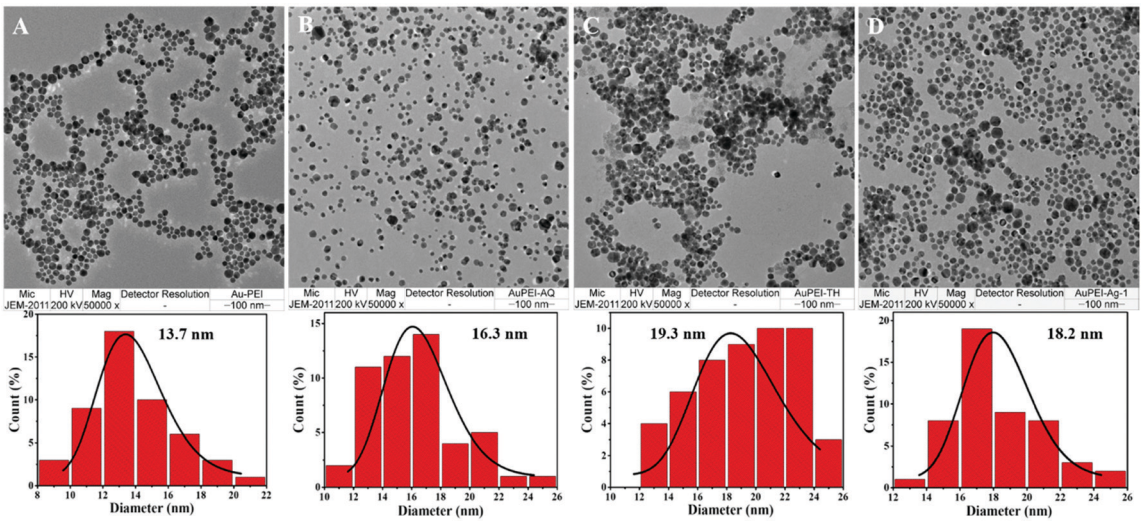

Fig. 1 TEM images and histograms of (A) PEI-AuNPs, (B) AQ-anti-MUC1-PEI-AuNPs, (C) TH-anti-CA15-3-PEI-AuNPs, and (D) Ag^+-anti-HER2-PEI-AuNPs.

metal ions, the diameters of AQ-anti-MUC1-PEI-AuNPs (Fig. 1B), TH-anti-CA15-3-PEI-AuNPs (Fig. 1C), and Ag^{+}-anti-HER2-PEI-AuNPs (Fig. 1D) are *ca.* 16.3, 19.3, and 18.2 nm, respectively. It is found that the diameters of the three conjugation systems increase with a negligible aggregation when compared with that of the PEI-AuNPs. This result suggests that three types of redox species-antibody-PEI-AuNP bioconjugates are successfully prepared. Moreover, when the products were deposited onto a three-electrode array, the surface morphologies of bare SPCE and AQ-anti-MUC1-PEI-AuNPs-, TH-anti-CA15-3-PEI-AuNPs-, and Ag^{+}-anti-HER2-PEI-AuNPs-modified SPCEs are characterized using the SEM technique as presented in Fig. S4 (ESI†). The electrode surfaces modified with all redox species-antibody-PEI-AuNP bioconjugates provide a characteristic of PEI-AuNPs with a narrow distribution of granular PEI-AuNPs and negligible aggregation (Fig. S4B–D, ESI†), while the unmodified electrode shows no presence of PEI-AuNPs (Fig. S4A, ESI†). This result confirms that the conjugation of PEI-AuNPs is successfully applied onto the electrode surface.

Electrochemical properties of the antibody-conjugated PEI-AuNPs

The CV and EIS measurements are used to confirm the formation of the sensing surface employing our developed antibody-conjugated PEI-AuNPs without redox-active species and to monitor the stepwise fabrication process of the immunosensor. The measurements are undertaken with 3-SPCE arrays modified with different materials in contact with 0.010 M PBS (pH 7.4) containing 5.0 mM $[Fe(CN)_6]^{3-/4-}$ as shown in Fig. S5 (ESI†). CVs of bare SPCE and PEI-AuNPs-, antibody-PEI-AuNPs-, BSA/antibody-PEI-AuNPs-, and protein/BSA/antibody-PEI-AuNPs-modified SPCEs are presented in Fig. S5A (ESI†). The bare 3-SPCE array (curve a) exhibits a well-defined pair of reversible oxidation/reduction peaks of $[Fe(CN)_6]^{3-/4-}$. After being modified with PEI-AuNPs (curve b), the peak current increases obviously with a lowered peak-to-peak separation (ΔEp) value (*ca.* 0.160 V), as compared to a bare SPCE (*ca.* 0.270 V), illustrating an excellent ability of electron transfer of the AuNPs. When the captured antibodies are immobilized on PEI-AuNPs and the bioconjugates are modified on each SPCE of the array (curve c), the current response decreases gradually with the ΔEp value of 0.170 V, implying the successful binding of antibodies to PEI-AuNPs, because biomolecules can retard the transfer of electrons. Sequentially, the peak current continues to decrease after incubation of the antibody-PEI-AuNPs-modified SPCE with BSA due to the blockage of non-specific adsorption sites (curve d), and it decreases again due to the formation of immunocomplexes when antigens are added on the surface of the BSA/antibody-PEI-AuNPs-modified SPCE (curve e), which originates from the increment of the thickness of the insulating protein layers that obstructed the electron transfer at the interface. The result indicates that the immunocomplex is formed successfully, and antibody-PEI-AuNPs have a high ability to capture the target biomarkers as well as to form the sensing surface. Three kinds of antibody-PEI-AuNPs can be used in the next step to construct the electrochemical immunosensor.

Correspondingly, EIS is also employed to monitor the interfacial properties of the 3-SPCE electrode array during stepwise modifications (Fig. S5B, ESI†). To derive the charge transfer resistance value (R_{ct}), EIS spectra are fitted with a modified Randles circuit using PS Trace software. The semicircle diameter of the Nyquist plot is related to charge transfer resistance.[36] As shown in Fig. S5B (ESI†), the bare SPCE (curve a) shows a large semicircle diameter, suggesting a high R_{ct} value of *ca.* 519 Ω. Meanwhile, the SPCE array modified with PEI-AuNPs (curve b) shows a straight line, implying that the PEI-AuNPs have an influential drive in accelerating the electron transfer due to high conductivity and their large surface area.[37] Moreover, the surface areas of the bare SPCE and the PEI-AuNPs-modified SPCE are calculated using CVs at different scan rates by the Randles-Sevcik equation.[38] As a result, the electroactive surface areas of the bare SPCE and the PEI-AuNPs-modified SPCE are found to be 7.44 cm^2 and 13.70 cm^2, respectively, where the surface area is improved about approximately two fold. After the antibodies are attached to PEI-AuNPs and then the particles are modified on the SPCE array, the semicircle increases with R_{ct} of 21 Ω (curve c), as compared with that of the PEI-AuNPs-modified SPCE. A larger semicircle diameter with R_{ct} of 74 Ω is observed after blocking the SPCE array surface with BSA (curve d). The semicircle is further enlarged with R_{ct} of 103 Ω after antigens anchor on the sensing surfaces of the array due to immunoreaction (curve e). This is due to the larger obstruction effect of protein layers on the flow of electrons. Thus, the EIS measurements are consistent with the CV results, revealing the successful fabrication of the immunosensing interface.

Since the immunosensor can be constructed by direct deposition of the three kinds of developed redox probe-antibody-PEI-AuNPs onto a 3-SPCE array, its multiplex label-free detection is tested. Firstly, their well-separated voltammetric responses of the corresponding determined target analytes are required. In addition, the SWV technique is used to measure the electrochemical redox property of the redox-active species sitting on the prepared 3-SPCE array platform in 0.2 M acetate buffer (pH 5.0) as illustrated in Fig. S6 (ESI†). A 3-SPCE array containing PEI-AuNPs conjugated to anti-MUC1, anti-CA15-3, and anti-HER2 then bound with three different redox species, namely AQ-anti-MUC1-PEI-AuNP (curve a), TH-anti-CA15-3-PEI-AuNPs (curve b), and Ag^{+}-anti-HER2-PEI-AuNPs (curve c), respectively. They exhibit three corresponding distinct redox peaks, which can represent their own target biomarkers due to the reaction with surface-confined antibodies. The comparable and distinguishable signals of the three redox bioconjugates prepared by our developed condition are observed at −0.40 (position a), −0.15 (position b), and 0.35 mV (position c), respectively, in a single run. Hence, the potential differences in the peak position allow the simultaneous determination of three tumor markers.

Study of the fabrication steps and optimization of the conditions for electrochemical detection

Fig. 2 shows monitoring of the stepwise fabrication of the multiplex immunosensor employing a three-prepared redox species-antibody-PEI-AuNPs-modified 3-SPCE array. The SWV measurements are used to study the immobilization steps, which are carried out with the sensing surfaces in contact with 0.2 M acetate buffer (pH 5.0). The highest peak currents are observed for the 3-SPCE array after the deposition of the redox

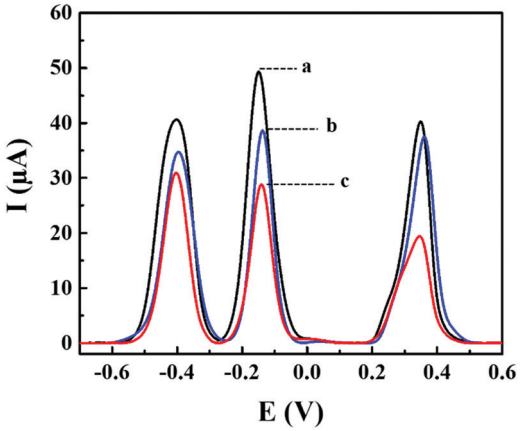

Fig. 2 SWV current responses of (a) the three-redox species-antibody-PEI-AuNPs-modified SPCE (b) after incubation with 0.05% BSA, and (c) after incubation with 5 ng mL^{-1} of MUC1 and HER2, and 5 U mL^{-1} of CA15-3, measured in 0.2 M acetate buffer (pH 5.0).

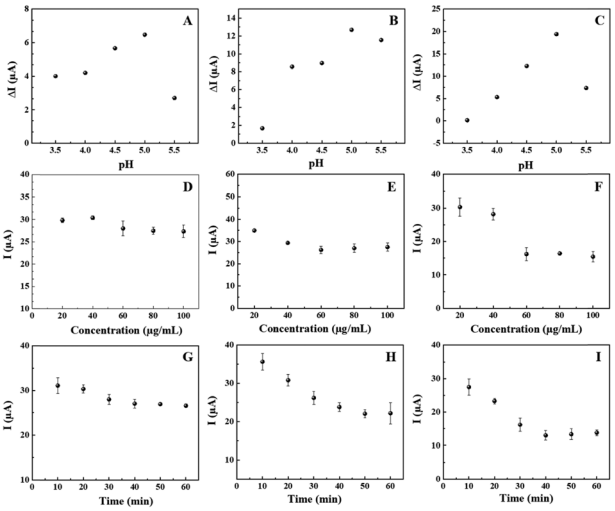

Fig. 3 Effect of pH on the detection based on the change of current (ΔI) between before and after binding with a solution containing 50 ng mL^{-1} MUC1 (A), 50 U mL^{-1} CA15-3 (B) and 50 ng mL^{-1} HER2 (C) and effect of concentrations of anti-MUC1 (D), anti-CA15-3 (E), and anti-HER2 (F) antibodies for fully binding on PEI-AuNPs and effect of incubation time of MUC1 (G), CA15-3 (H), and HER2 (I) for the complete immunoreaction.

bioconjugates (curve a). After blocking with 0.05% w/v BSA, all signals decrease (curve b). Subsequently, the current signals further decrease when antigens are added onto the surfaces (curve c). This is caused by the electrode-bound biomolecules, acting as a nonconductor, which greatly inhibits the corresponding redox reactions at the array electrode surfaces. Thus, it confirms that the fabrication process is feasible, and our redox species-antibody-PEI-AuNPs can be used for the label-free determination of multiple analytes, *i.e.*, MUC1, CA15-3, and HER2.

To obtain high sensitivity for the simultaneous determination of MUC1, CA15-3, and HER2, the pH value, antibody concentration, and antigen–antibody incubation time are optimized. The pH of the acetate buffer solution significantly affects the electrochemical behavior of the immunosensor because it influences the activity of the immobilized protein and the electrochemical activity and stability of redox-active species; AQ, TH, and Ag^{+}. Consequently, a series of acetate buffer solutions (0.20 M) at different pH values (3.5–5.5) are prepared and used as operating electrolytes to obtain the analytical response through SWV, and the current differences (ΔI) from the SWVs before and after incubation of the immunosensor with biomarker solution are compared. The sensor is constructed by employing three kinds of bioconjugates on individual SPCEs. The bioconjugates are prepared using 60 μg mL^{-1} antibodies, and the immunoreaction time used is 30 min. Fig. 3A–C shows that the ΔI value increases when increasing the pH value from 3.5 to 5.0 and then decreases at a higher pH value. Highly acidic or alkaline pH will lead to dissociation of the antibody–antigen complex, causing smaller ΔI values. The best performance of the immunosensor is achieved with pH 5.0. So, this pH value is chosen for the next study and the further simultaneous detection due to the provision of the stability of redox reactivity and the preserved bioactivity of antibody/antigen.

To achieve the highest protein loading, the effect of the concentrations of the anti-MUC1, anti-CA15-3, and anti-HER2 antibodies are investigated, and the concentrations are varied from 20 to 100 μg mL^{-1}. pH 5.0 and the time of 30 min to complete immunoreaction were used. After incubation with target biomarker solutions, the intensities of SWV response peaks reduce due to forming immunocomplexes. It can be seen in Fig. 3D–F that the currents start to become constant at the concentration of antibodies of 60 μg mL^{-1}. This is caused by the saturation of loaded antibodies on a 3-SPCE array. Thus, antibody concentrations of 60 μg mL^{-1} are used for further investigating the optimal incubation time for the immunoreaction.

Additionally, the incubation time for the completion of antibody-antigen binding is another critical parameter in the construction of the immunosensor. When antigens reach the surface-confined antibodies that are modified on the surface of the immunosensor, they need certain times to form immunocomplexes completely. Thus, the effect of incubation time is investigated with the time range of 10–60 min by incubating the sensing surfaces with 50 ng mL^{-1} MUC1 and HER2, and 50 U mL^{-1} CA15-3. After adding the corresponding biomarker antigens, the current responses of AQ (Fig. 3G), TH (Fig. 3H), and Ag^{+} (Fig. 3I) rapidly decrease with the increment of incubation time and tend to level off after 40 min, indicating the saturated formation of antigen–antibody complexes. Therefore, the immunoreaction time of 40 min is selected for multiplex detection of MUC1, CA15-3, and HER2.

Simultaneous detection and analytical performance of the biosensor

PEI-AuNPs conjugated to anti-MUC1, anti-CA15-3, and anti-HER2 using three redox species, giving distinguishable signals, are deposited on a 3-SPCE array and used for simultaneously detecting the clinically relevant breast cancer biomarkers (MUC1, CA15-3, and HER2). Redox species AQ (for MUC1), TH (for CA15-3), and Ag^{+} (for HER2) distinguish the analytical signals at different voltages when the BSA/antibody-PEI-AuNPs-modified electrode

array is exposed to varying concentrations of CA15-3 (0.10–100 U mL^{-1}), and MUC1 and HER2 antigens (0.10–100 ng mL^{-1}). SWV peak current responses with increasing concentrations of respective antigens are represented in Fig. 4A. It is noted that the current responses decrease gradually with increasing concentrations of the biomarkers. Antibodies and antigens being protein molecules are electrochemically inactive; therefore, the layers of their immunocomplexes on electrodes easily block electrochemical reactions of redox species on the electrode array surface. Furthermore, linear calibration plots of % decreasing currents *versus* the logarithm of the concentrations of corresponding biomarkers;[39,40] MUC1, CA15-3, and HER2 in the ranges of 0.10–100 ng mL^{-1}, 0.10–100 U mL^{-1}, and 0.10–100 ng mL^{-1}, respectively, are shown in Fig. 4B–D, respectively.

The limits of detection (LODs) for all are calculated from 3SD/slope.[41] The estimated LODs of MUC1, CA15-3, and HER2 are 0.53 ng mL^{-1}, 0.21 U mL^{-1}, and 0.50 ng mL^{-1}, respectively. With considering the applicability of our multiplex sensor, the cut-off values of MUC1, CA 15-3, and HER2 are 10–15 ng mL^{-1},[42] 25 U mL^{-1},[43] and 15 ng mL^{-1},[43] respectively. The LODs of this strategy are clearly lower than the cut-off values; therefore, the sensitivity of the developed immunosensor is exceedingly satisfied and can be used for diagnosing and monitoring patients with breast cancer.

Meanwhile, there is no study reported about the multiplex detection of three biomarkers like in our sensing system. Thus, we have compared the performance of this present work to other works reported for the individual or simultaneous detections of MUC1, CA15-3, and/or HER2, as listed in Table S1 (ESI†). The calibration ranges and LODs of this immunosensor are better than the previous studies in Entries 1 and 3. The sensors reported in Entries 2, 4, and 5 show much lower LODs than those of our work; however, Entry 5 cannot perform the simultaneous detection and reveals a shorter dynamic range. Although Entries 2 and 4 present wider calibration ranges and better LODs, they are demonstrated for detections of single biomarkers employing single redox probes, which perhaps would not have a problem from interfering response and cross-reactivity like a multiplex sensor. Moreover, Entry 2 is fabricated with a complicated procedure. Our sensor also displays wider dynamic ranges than those of the detections of CA 15-3, HER2, and MUC1 in Entries 1, 3, and 5. It is plausible that the convenient fabrication and simplicity of the proposed immunosensor make it much more attractive. Additionally, the concentration ranges of this work cover practical applications.

Evaluation of the reproducibility, cross-reactivity, specificity, and stability of the immunosensor

Reproducibility is an essential factor in practical applications for the successful fabrication of a multiplex immunosensor giving an accurate assay. In order to evaluate the reproducibility of the immunosensor, the seven freshly prepared modified 3SPCE electrode arrays before and after incubation with 5 ng mL^{-1}/U mL^{-1} MUC1, CA15-3, and HER2 are employed to study this parameter. As shown in Fig. 5, the blank responses for all cases are higher than those after binding with the biomarker targets. The current differences as analytical responses are *ca.* 5.50, 10.84, and 15.86 μA (% decreasing currents of *ca.* 16.11, 27.54, and 44.42) for MUC1, CA15-3, and HER2, respectively. The relative standard deviations (RSDs) of the sensor are 1.82%, 3.58%, and 3.53% for blank measurements, namely the responses of the BSA/anti-MUC1-AQ-PEI-AuNPs-, BSA/anti-CA15-3-TH-PEI-AuNPs-, and BSA/anti-HER2-Ag-PEI-AuNPs-modified 3-SPCE array, respectively, and 4.5%, 3.9%, and 6.5% for multiplex detection of 5 ng mL^{-1}/U mL^{-1} MUC1, CA15-3, and HER2, respectively, indicating acceptable reproducibility of our developed immunosensor.

Moreover, the applicability of the sensor is limited by interfering signals between the detections of different antigens.

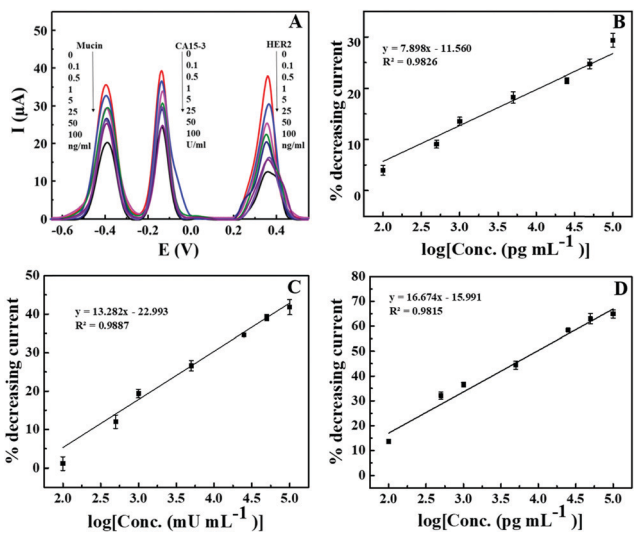

Fig. 4 SWV responses (A) of the immunosensor for different concentrations of the multiple targets and corresponding calibration curves for MUC1 (B), CA15-3 (C), and HER2 (D).

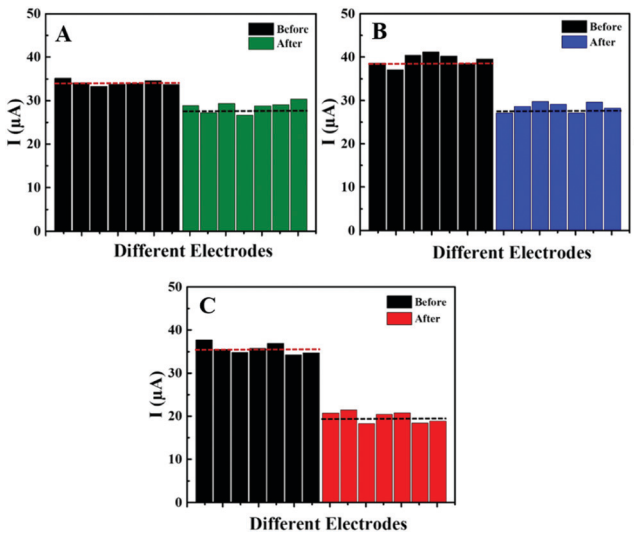

Fig. 5 Reproducibility of the electrochemical immunosensor before and after incubation with a solution containing 5 ng mL^{-1} MUC1, RSD = 4.5% (A), 5 U mL^{-1} CA15-3, RSD = 3.9% (B), and 5 ng mL^{-1} HER2, RSD = 6.5% (C).

In general, in a single electrode, the multiplex ability in the detection is high with the sandwich-type fashion while the label-free configuration faces the unidentified blockage of electrochemical processes, caused by concerted immunoreactions. In order to avoid interfering signals, the multiplex detection based on the label-free manner with a spatial area between each sensing surface for assay of a single antibody-antigen pair overcomes this drawback. The individual sensing surfaces attached with different kinds of antibodies reveal the detection of different single targets and allows simultaneous detection within a single run. In our study, we demonstrate three SPCE surfaces of the electrode array having different antibodies attached with different corresponding redox-active species for simultaneous label-free detection. The cross-reactivity of the multiplex electrochemical immunosensor is investigated as shown in Fig. S7 (ESI†). It is found that the immunosensors in the presence of the corresponding target biomarkers/antigens show an obvious decrease in SWV responses at the corresponding peak position. Single and multiplex detections in the multiplex immunosensor are insignificantly different, suggesting no cross-reactivity. Therefore, a simultaneous multianalyte immunoassay can be performed in a single run using the proposed sensor.

The specificity of the immunoassay is evaluated by incubating the immunosensor with the biomarker target solutions without and with the presence of some potential interferents contained in the human body such as IgG, AFP, GM2AP, IL-15, AA, DA, and Glu. Although some ultratrace and/or cancer-related interferences such as AFP, GM2AP, and IL-15 are not involved in this study, they are used as model interfering proteins. Moreover, IgG, GM2AP, and Glu are generally found at detectable levels in human body fluid. The relative responses of all (responses after incubating targets solution with the absence of the interferences as 100% relative currents) are shown in Fig. 6. When the immunosensor is added with the target solutions with the different spiked interferences (500 ng mL^{-1}), the results are compared with the measurement

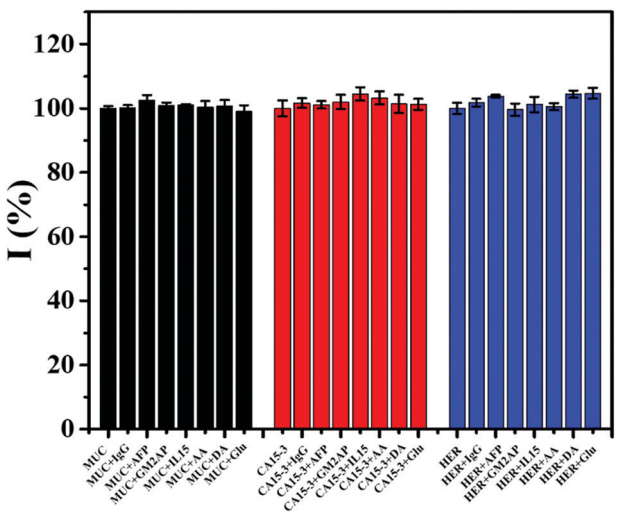

Fig. 6 Interference study of the proposed immunosensor for the simultaneous detection of MUC1 (5 ng mL^{-1}), CA15-3 (5 U mL^{-1}), and HER2 (5 ng mL^{-1}) and mixed with different interferents (500 ng mL^{-1}).

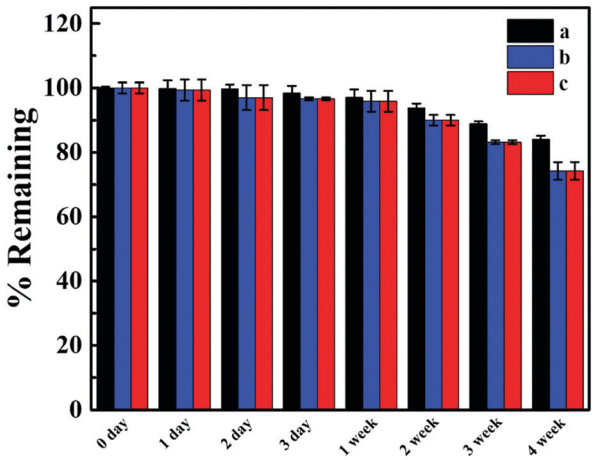

Fig. 7 Stability study of the electrochemical immunosensor for the simultaneous detection of (a) MUC1 (5 ng mL^{-1}), (b) CA15-3 (5 U mL^{-1}), and (c) HER (5 ng mL^{-1}).

for only 5 ng mL^{-1}/U mL^{-1} MUC1, CA15-3, and HER2 antigens. It is seen that even the target solution contains a very high concentration of the interferences, the differences in electrochemical responses are less than 5%, indicating the good selectivity in detecting three breast cancer biomarkers. Furthermore, the storage stability of our dye/metal ion-antibody-PEI-AuNPs bioconjugates for the construction of the proposed immunosensor is also tested, as depicted in Fig. 7. The materials are stored at a temperature of 4 °C for stability tests over four weeks. After storage at certain periods, the sensors are freshly prepared using deposition of the bioconjugates on 3-SPCE arrays. The peak responses are recorded after the sensing surfaces are incubated with related biomarker antigens. After two weeks, the current responses of all sensors retain 90% of their initial currents, thus giving acceptable stability.

Application in the analysis of three breast cancer biomarkers in human serum

The reliability and feasibility of the proposed immunosensor for the detection of multiple biomarkers in real sample analysis are investigated. The developed immunosensing platform is applied to detect three breast cancer biomarkers in a human serum sample. The 50-diluted serum solutions are spiked with five different concentrations of target antigens (0.50, 1.00, 5.00, 25.00, and 50.00 ng mL^{-1} for MUC1 and HER2 and 0.50, 1.00, 5.00, 25.00, and 50.00 U mL^{-1} for CA15-3), which are employed for the recovery study. The results are presented in Table 1. The recoveries of the MUC1, CA15-3, and HER2 detections in the human serum sample by our multiplex immunosensor are obtained in an acceptable range of 96.69–104.95%, 96.68–104.05%, and 101.12–105.48%, respectively, indicating satisfactory accuracy in the simultaneous detection in the sample matrix. Therefore, this immunosensor has the possibility for application in clinical diagnostics. The successful determination of MUC1, CA15-3, and HER2 at once would serve precise and accurate breast cancer diagnosis, and our strategy will be extended to developing other kinds of multiplex cancer sensors in the future.

Table 1 Assay result (Mean ± SD, n = 3) of human serum sample by the proposed label-free electrochemical immunosensor

	Added			Proposed method			Recovery (%)		
Sample No.	MUC1 (ng mL^{-1})	CA15-3 (U mL^{-1})	HER2 (ng mL^{-1})	MUC1 (ng mL^{-1})	CA15-3 (U mL^{-1})	HER2 (ng mL^{-1})	MUC1	CA15-3	HER2
1	0.50	0.50	0.50	0.48 ± 0.01	0.51 ± 0.02	0.51 ± 0.02	96.69	102.92	101.12
2	1.00	1.00	1.00	1.02 ± 0.02	0.95 ± 0.02	1.03 ± 0.01	102.00	95.29	102.88
3	5.00	5.00	5.00	4.93 ± 0.06	4.83 ± 0.11	5.27 ± 0.10	98.66	96.68	105.48
4	25.00	25.00	25.00	24.49 ± 0.39	26.01 ± 0.74	26.27 ± 0.50	97.97	104.05	105.08
5	50.00	50.00	50.00	52.48 ± 1.01	51.21 ± 1.36	51.58 ± 0.82	104.95	102.42	103.16

Conclusions

A novel label-free electrochemical immunosensor for the simultaneous detection of three breast cancer biomarkers (MUC1, CA 15-3, and HER2) is constructed based on redox species-antibody-conjugated PEI-AuNPs. The immunosensor relies on the electrochemical signals of AQ, TH, and Ag^{+} for indicating the three different biomarkers, at the potentials of −0.39, −0.13, and 0.36 V, respectively. PEI-AuNPs not only increase the conductivity but also provide a large surface area for the loading of both antibodies and redox species. The developed immunosensor can simultaneously detect the three tumor markers, which helps to reduce the analysis time and cost and improve the precision of clinical analysis. The immunosensor provides good multiplex ability, satisfactory reproducibility, high specificity, and excellent long-term storage stability. The results suggest that the designed immunosensor has great potential for the simultaneous detection of breast cancer biomarkers in real samples and can be applied in developing the clinical detection of other tumor markers.

Author contributions

Kulrisa Kuntamung: investigation, writing – original draft. Jakmunee: writing – review & editing. Kontad Ounnunkad: conceptualization, methodology, validation, resources, writing – original draft, writing – review & editing, visualization, supervision, project administration, funding acquisition.

Conflicts of interest

There are no conflicts to declare.

Acknowledgements

K. K. would like to thank an award of the Science Achievement Scholarship of Thailand (SAST). This research work was supported by Chiang Mai University (CMU). The authors gratefully acknowledge the Graduate School (CMU), Research Center on Chemistry for the Development of Health Promoting Products from Northern Resources, Center of Excellence for Innovation in Chemistry (PERCH-CIC), Center of Excellence in Materials Science and Technology, and Department of Chemistry, Faculty of Science, CMU. We would like to thank the Program Management Unit for Human Resources & Institutional Development, Research and Innovation, Office of National Higher Education Science Research and Innovation Policy Council (NXPO) [Grant Number B16F640001] for financial support.

References

1 R. L. Siegel, K. D. Miller and A. Jemal, *Ca-Cancer J. Clin.*, 2020, **70**, 7–30.
2 F. Bray, *et al.*, *Ca-Cancer J. Clin.*, 2018, **68**, 394–424.
3 G. N. Sharma, *et al.*, *J. Adv. Pharm. Technol. Res.*, 2010, **1**, 109–126.
4 L. Nemchek, *Clin. J. Oncol. Nurs.*, 2018, **22**, E127–E133.
5 Z. Kakushadze, R. Raghubanshi and W. Yu, *Data*, 2017, **2**, 30.
6 T. Feng, *et al.*, *J. Mater. Chem. B*, 2016, **4**, 990–996.
7 Q. Rong, F. Feng and Z. Ma, *Biosens. Bioelectron.*, 2016, **75**, 148–154.
8 A. M. Kabel, *J. Oncol.*, 2017, **3**, 5–11.
9 S. Rauf, *et al.*, *Anal. Biochem.*, 2018, **545**, 13–19.
10 R. Hu, *et al.*, *Biosens. Bioelectron.*, 2014, **53**, 384–389.
11 Y. He, *et al.*, *Nanoscale*, 2012, **4**, 2054–2059.
12 J. Wu, *et al.*, *Trac, Trends Anal. Chem.*, 2007, **26**, 679–688.
13 A. Osman, *et al.*, *Breast Cancer Curr. Res.*, 2016, **1**, 114.
14 M. Araz, *et al.*, *Curr. Probl. Cancer*, 2019, **43**, 115–122.
15 S. Yang, *et al.*, *Sens. Actuators, B*, 2018, **258**, 796–802.
16 N. Liu, *et al.*, *J. Mater. Chem. B*, 2014, **2**, 3292–3298.
17 Z. Ma and N. Liu, *Expert Rev. Mol. Diagn.*, 2015, **15**, 1075–1083.
18 R. Laocharoensuk, *Electroanalysis*, 2016, **28**, 1716–1729.
19 H. Wang and Z. Ma, *Sens. Actuators, B*, 2018, **256**, 402–407.
20 Y. Lv, *et al.*, *ACS Sens.*, 2018, **3**, 1362–1367.
21 Z. Cui, *et al.*, *Anal. Chim. Acta*, 2014, **807**, 44–50.
22 X. Jia, *et al.*, *Biosens. Bioelectron.*, 2014, **53**, 160–166.
23 X. Chen and Z. Ma, *Biosens. Bioelectron.*, 2014, **55**, 343–349.
24 X. Chen, *et al.*, *Biosens. Bioelectron.*, 2013, **50**, 356–361.
25 H. Filik and A. A. Avan, *Talanta*, 2019, **205**, 120153.
26 J. Qian, *et al.*, *Biosens. Bioelectron.*, 2011, **28**, 314–319.
27 H. Qi, *et al.*, *Analyst*, 2012, **137**, 393–399.
28 F. Y. Kong, *et al.*, *Chem. Commun.*, 2013, **49**, 1052–1054.
29 T. Xu, *et al.*, *Biosens. Bioelectron.*, 2014, **56**, 174–179.
30 L. Wang, F. Feng and Z. Ma, *Sci. Rep.*, 2015, **5**, 16855.
31 T. Xu, *et al.*, *Biosens. Bioelectron.*, 2015, **70**, 161–166.
32 D. Tang, *et al.*, *Biosens. Bioelectron.*, 2013, **46**, 37–43.
33 S. A. Bansal, *et al.*, *Nanoscale Adv.*, 2020, **2**, 3764–3787.
34 R. Thiramanas and R. Laocharoensuk, *Microchim. Acta*, 2016, **183**, 389–396.

35 T. Putnin, *et al.*, *Microchim. Acta*, 2019, **186**, 305.
36 H. Zhang, *et al.*, *J. Electrochem. Soc.*, 2020, **167**, 027515.
37 Z. Huang, *et al.*, *Int. J. Nanomed.*, 2017, **12**, 3049–3058.
38 S. P. Mundinamani and M. K. Rabinal, *IOSR J. Appl. Chem.*, 2014, **7**, 45–52.
39 C. Thunkhamrak, *et al.*, *Talanta*, 2020, **208**, 120389.
40 J. Upan, *et al.*, *Electrochim. Acta*, 2020, **349**, 136335.
41 K. Kuntamung, *et al.*, *Analyst*, 2021, **146**, 2203.
42 Method of human blood serum testing for oncomarker muc1, https://patents.google.com/patent/RU2338200C1/en, (accessed April 2021).
43 R. C. B. Marques, *et al.*, *Sens. Actuators, B*, 2018, **255**, 918–925.